J. Fluid Mech. (1973), *vol.* 60, *part* 3, *pp.* 433–457
Printed in Great Britain

The stability of axisymmetric free shear layers

By MARTIN LESSEN AND PAWAN JIT SINGH
Department of Mechanical and Aerospace Sciences, University of Rochester, New York

(Received 25 September 1972)

The stability of laminar axisymmetric jets and wakes, the two prominent examples of free shear layers, is investigated with respect to linear azimuthally periodic disturbances. The complete viscous disturbance equations are integrated numerically and the eigenvalues are obtained by matching the numerically advanced solutions to the asymptotic solutions at a large radius. Both spatial and temporal stability are examined for inviscid and viscid flows. It is found that the critical Reynolds number for the jet and the wake are not much different while the amplification rates for the wake become considerably greater than those for the jet as the Reynolds number increases. The axisymmetric shear-layer flows also seem to be more stable than the corresponding plane flows.

1. Introduction

The stability of plane free shear layers has been investigated by numerous authors for many years; however, the analysis of the stability of axisymmetric free shear layers has only received scant attention. It is felt that there has been a tacit assumption that the difference between plane and cylindrical geometry does not have a significant effect on the stability characteristics of such flows; such an assumption is not fully borne out by the present investigation. Jets and wakes are two prominent examples of axisymmetric free shear layers which occur commonly. It is necessary to have a knowledge of the stability, transition and transport properties of such flows. Such information is useful, for example, in chemical reactor and combustor design in the case of jets and for drag calculations in the case of wakes.

Batchelor & Gill (1962) presented a detailed analytical treatment for the inviscid instability of free axisymmetric flows, in particular jets. Rayleigh (1892) determined that the necessary condition for the existence of amplified disturbances in such flows is that

$$Q(r) = rU'/(n^2+\alpha^2 r^2) \tag{1.1}$$

should have a numerical maximum somewhere in the fluid. This condition is an analogue of the requirement of a maximum of mean vorticity for plane parallel flows. In Rayleigh's work, α and n are respectively the axial and azimuthal wavenumbers of the Fourier components of the disturbance, $U(r)$ is the mean flow velocity and r is the radial co-ordinate. This condition defines the range of the parameters α and n for which the flow can be unstable. Batchelor & Gill,

using an even more restrictive condition, showed that there is one and only one neutral disturbance ($\alpha \neq 0$) for the far jet profile ($U = 1/(1+r^2)^2$) and that it is possible only when $n = 1$. They also computed the neutral wavenumber for this profile and provided the amplification curves for a top-hat jet.

The results of the experimental work regarding the stability of submerged circular jets have not been conclusive. Villu (1962) obtained a critical Reynolds number for instability of about 10. Reynolds (1962) reported presumably unpublished results by Schade, who found that a long, nearly rectilinear jet could be maintained at a Reynolds number of several hundred. His own investigation inspired by this contradiction revealed several modes of instability for Reynolds numbers R from nearly 10 onwards. In particular, he found axisymmetric condensations over a range of R from 50 to 250 and sinuous undulations of long wavelength at an R near 100. As the unstable axisymmetric disturbances are ruled out by the inviscid theory, Gill (1962) suggested that the growth of small but finite disturbances is responsible for the condensations in the viscous fluid. McNaughton & Sinclair (1966) carried out a similar experiment with varying sizes of jet orifices and containing vessels over a Reynolds-number range of 100–28 000 and reported modes of breakdown similar to those obtained by Reynolds. They presented their results in the form of a relation for the laminar length and it is difficult to obtain a critical Reynolds number from their investigation. Kambe (1969) studied the stability of the jet with a parabolic profile by asymptotic methods in the limits of small αR and large αR and calculated a critical Reynolds number of 32·8 for the sinuous mode. His examination showed that the amplified disturbances did not exist for the rotationally symmetric ($n = 0$) mode and that the $n = 1$ mode was more unstable than the $n = 2$ mode.

Sato & Okada (1966) made an experimental study of the instability and transition of the wake behind an axisymmetric slender body at high Reynolds number. Their measurements indicated the existence of a laminar wake past the tip of the body which gradually developed into a turbulent wake. It was different from the wake produced by bluff bodies, where the turbulent eddies arising at the separation point dominate the further flow and a laminar wake develops gradually at relatively large distances downstream as the Reynolds number decreases with the distance. The measured mean velocity profile resembled the theoretical similarity profile for a considerable distance. They reported a good comparison between their experimental results and the theoretical calculations based on the linearized inviscid disturbance equations. Using the condition specified by Batchelor & Gill, they found that neutral disturbances could exist only for the $n = 1$ and $n = 2$ modes; however, their computations revealed that only the $n = 1$ mode was unstable and they also experimentally observed the effect of helical disturbances on the stability. Physically the sinuous mode tends to flute the whole mass of the fluid like a kinked wire and allows non-zero velocities at the axis unlike other modes. On the basis of the results of the above and of other axisymmetric flow stability analyses, it seems most likely that the $n = 1$ mode will be most unstable. So we have carried detailed calculations only for this mode (see appendix A).

2. Mean flow profiles

The axially symmetric jet

We consider a jet of incompressible fluid emerging from a small circular orifice into an infinite mass of the same uniform fluid without azimuthal swirl. Schlichting (1955, p. 181) calculated the velocity profile of such a jet using boundary-layer theory and assuming a similarity profile away from the orifice. Landau (1943) later derived the same profile by using the complete Navier–Stokes equations for the case of large momentum flux. He determined the stream function for a steady jet due to a force applied at a point the origin, in an unbounded fluid. The angular spread of the jet can be related to the force M:

$$3M/\pi\rho\nu^2 \sim 32/\theta_0^2$$

if M is large. ρ is the density of the fluid, ν is the kinematic viscosity and θ_0 is the value of the polar angle at which streamlines are least distant from the direction of the force at the origin. The axial velocity U_a is given by

$$U_a = \frac{8\nu x r_0^2}{(r^2+r_0^2)^2} = \frac{U_0}{(1+r^2/r_0^2)^2}, \tag{2.1}$$

where x is the axial distance from origin, $U_0 = 8\nu x/r_0^2$ is the characteristic velocity and $r_0 = x\tan\theta_0$ represents the spread of the jet and is used as the characteristic length. The Reynolds number

$$R = \frac{U_0 r_0}{\nu} = \frac{8x}{r_0} \sim \frac{8}{\theta_0} \text{ for small } \theta_0.$$

So with U_0 and r_0 as the velocity and length scales respectively, the non-dimensional velocity distribution for the jet is $U = 1/(1+r^2)^2$. Landau's solution is also valid at a distance if the jet emerges from a finite orifice instead of a point source, the solution being the zeroth-order term in a series expansion in powers of the ratio of the orifice dimensions to the distance from the source.

We assume that the flow is locally parallel. This will be valid if $V/U \ll 1$, where V is the radial velocity. For the jet

$$V/U = \begin{cases} 0 & \text{at } r = 0, \\ O(\theta_0) & \text{at } r = r_0, \end{cases}$$

which is small in our approximation of M large and thus θ_0 small. Also U_0 and r_0 should not vary significantly over a wavelength although R remains constant for the jet with increasing axial distance. This requirement is satisfied if $\alpha x \gg 1$ or if $\frac{1}{8}\alpha r_0 R \gg 1$ as

$$r_0 = x\tan\theta_0 \sim 8x/R.$$

It will be convenient to relate the Reynolds number to the volume flux Q, and the area of orifice A, which are measurable quantities. This relation depends upon the velocity distribution at the orifice. It can be easily deduced (see Batchelor & Gill) that

$$R = \begin{cases} (4/\pi A)^{\frac{1}{2}} Q/\nu & \text{for a parabolic velocity distribution,} \\ (3/\pi A)^{\frac{1}{2}} Q/\nu & \text{for a uniform velocity distribution.} \end{cases}$$

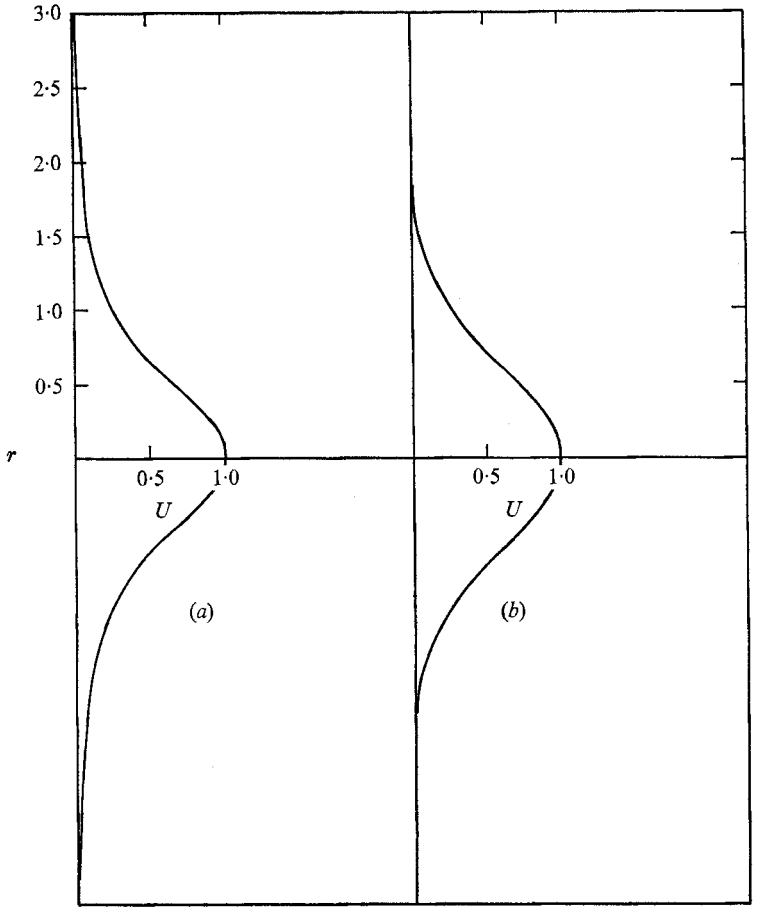

FIGURE 1. The mean velocity profiles. (*a*) Axisymmetric jet. (*b*) Axisymmetric wake.

Thus if R_0 is the Reynolds number based on the mean velocity Q/A with the diameter of the orifice as the characteristic length, $R = R_0$ and $R = \frac{1}{2} \times 3\frac{1}{2} R_0$ for parabolic and uniform velocity distributions respectively.

The axially symmetric wake

There are two velocity scales for the wake: one is the uniform velocity away from the wake region and the other is related to the velocity defect $U_s = U_\infty - U$, where U is the velocity distribution in the wake region. The velocity defect distribution is given by (Rosenhead 1963, p. 455)

$$U_s = \frac{C}{x} \exp\left(-\frac{U_\infty r^2}{4\nu x}\right), \tag{2.2}$$

where C is a constant related to the drag experienced by the body and x is the axial distance from the origin of the wake. If we choose to non-dimensionalize the quantities by using the velocity scale $U_0 = C/x$, which is the maximum value

	m	n	$m+n$
Laminar jet	-1	1	0
Laminar wake	-1	$+\frac{1}{2}$	$-\frac{1}{2}$

TABLE 1. Figure 1 shows the mean velocity profiles for the jet and the wake

of the velocity defect, and a length scale r_0 defined as the radial distance at which the velocity defect is one-quarter of its greatest value at the axis, (2.2) reduces to

$$U_s = \exp(-ar^2), \quad \text{where} \quad a = 1{\cdot}386, \quad r_0 = (4\nu x a/U_\infty)^{\frac{1}{2}}. \tag{2.3}$$

Thus the non-dimensional velocity distribution in the wake region is found to be

$$U = q - \exp(-ar^2), \quad \text{where} \quad q = U_\infty/U_0. \tag{2.4}$$

Again the requirement for unidirectional flow is that $\alpha x \gg 1$.

The value of q varies with U_0, which depends on the axial distance x, and so the stability problem would have to be solved separately for each particular value of q. However, if α is real as in temporal stability analysis, the axial variation of U will only cause axial variation of the real part of the wave speed c (leaving $U-c$ same) and will not affect the amplification rate αc_i. The inversion of U can be accounted for by realigning the co-ordinates. So we have adopted the Gaussian profile $U = \exp(-ar^2)$ for our analysis, which does not change the temporal growth rates and varies the frequency. However spatial growth rates will vary with q and a general analysis cannot be presented. We have solved the spatial stability problem for the Gaussian profile to present a comparison with the corresponding problem for the jet in an attempt to study the effect of profile variation.

The velocity scale U_0 and length scale r_0 vary with x to maintain the similarity of the profile for non-parallel flows. If $U_0 \propto x^m$, $r_0 \propto x^n$ and so $R \propto x^{m+n}$, m and n vary as in table 1 for the above profiles.

3. Small disturbance equations

The flow of an incompressible fluid in the absence of external forces is governed by the following equations:

$$\nabla . \mathbf{u}^* = 0, \tag{3.1}$$

$$\frac{\partial \mathbf{u}^*}{\partial t} + (\mathbf{u}^* . \nabla)\mathbf{u}^* = -\frac{\nabla p^*}{\rho^*} + \nu \nabla^2 \mathbf{u}^*, \tag{3.2}$$

where $\mathbf{u}^* = \mathbf{u}^*(\mathbf{x}^*, t) = (u_x^*, u_r^*, u_\phi^*)$ and $\mathbf{x}^* = (x^*, r^*, \phi^*)$ in cylindrical co-ordinates.

The above equations can be non-dimensionalized with respect to a velocity scale U_0 and a length scale r_0. The resulting equations only differ in that ν is replaced by $1/R$ in (3.2), where R is the Reynolds number, given by $U_0 r_0/\nu$. Let the non-dimensional quantities be represented by eliminating the asterisks in (3.1) and (3.2). The velocity field $\mathbf{u}$ can be assumed to be the sum of an original

steady flow $\mathbf{U}(\mathbf{x})$ and an infinitesimal disturbance $\mathbf{u}'(\mathbf{x},t)$; this substitution in (3.1) and (3.2) yields the conventional linearized disturbance equations.

In the case of parallel flows, the undisturbed flow velocity has only an axial component. For the axisymmetric jet and the wake, we shall refer to it as $U(r)$. The finite energy disturbance quantities can be Fourier analysed and we assume the following normal-mode analysis:

$$\left.\begin{aligned} u'_x &= F(r)\exp[i\alpha(x-ct)+in\phi], \\ u'_r &= iG(r)\exp[i\alpha(x-ct)+in\phi], \\ u'_\phi &= H(r)\exp[i\alpha(x-ct)+in\phi], \\ P' &= P(r)\exp[i\alpha(x-ct)+in\phi], \end{aligned}\right\} \tag{3.3}$$

where P' is the kinematic pressure disturbance and F, G, H and P are complex amplitude functions. α and n are the axial and azimuthal wavenumbers respectively and c is the complex phase velocity. $\omega = \alpha c$ represents the frequency of the waves. The radial velocity amplitude function is displaced from the other velocity and pressure amplitude functions by a phase angle of $\frac{1}{2}\pi$, which results in cleaner disturbance equations; the incentive to do so is provided by the linearized continuity equation.

Substitution of (3.3) in the linearized equation yields

$$\alpha F + G' + G/r + nH/r = 0, \tag{3.4}$$

$$\alpha(U-c)F + U'G + \alpha P = \frac{1}{i\bar{R}}\left[F'' + \frac{1}{r}F' - \left(\alpha^2 + \frac{n^2}{r^2}\right)F\right], \tag{3.5}$$

$$\alpha(U-c)G - P' = \frac{1}{i\bar{R}}\left[G'' + \frac{1}{r}G' - \left(\alpha^2 + \frac{n^2+1}{r^2}\right)G - \frac{2n}{r^2}H\right], \tag{3.6}$$

$$\alpha(U-c)H + \frac{nP}{r} = \frac{1}{i\bar{R}}\left[H'' + \frac{1}{r}H' - \left(\alpha^2 + \frac{n^2+1}{r^2}\right)H - \frac{2n}{r^2}G\right], \tag{3.7}$$

where primes denote derivatives with respect to r.

The boundary conditions differ for various azimuthal modes and are governed by the requirement that the amplitudes F, G, H and P be bounded and go asymptotically to zero at $r = \infty$. The boundary conditions are given by

$$\begin{aligned} G(0) + H(0) = 0, \quad F(0), P(0) \text{ finite} \quad &\text{for} \quad n = 0, \\ F(0) = P(0) = 0, \quad G(0) + H(0) = 0 \quad &\text{for} \quad n = 1, \\ F(0) = G(0) = H(0) = P(0) = 0 \quad &\text{for} \quad n > 1, \\ F(\infty) = G(\infty) = H(\infty) = P(\infty) = 0 \quad &\text{for all } n. \end{aligned}$$

However, not all the boundary conditions are independent. As will be shown later, the disturbance equations can be transformed into a set of six first-order equations and thus only six boundary conditions are required for the closure of the problem.

The disturbance equations along with the homogeneous boundary conditions constitute an eigenvalue problem involving the parameters α, R, c and n. If α is real and $c = c_r + ic_i$, equation (3.3) shows that the disturbances will grow with

time if $c_i > 0$ and will decay if $c_i < 0$. The neutral disturbances are characterized by $c_i = 0$. If both α and c are complex and ω is real, the disturbances will grow as $e^{-\alpha_i x}$ in the axial direction. The criterion for spatial stability not only involves the direction in which the travelling waves are amplified but also the direction in which the wave energy is convected, determined by the sign of the group velocity c_g defined as $\partial\omega/\partial\alpha_r$, where $\alpha_r = \mathrm{Re}\,\alpha$. If $\alpha_i < 0$ and $c_g > 0$, i.e. energy is carried in the positive x direction, or if $\alpha_i > 0$ and $c_g < 0$, the flow is unstable. If $\alpha_i > 0$ and $c_g > 0$ or if $\alpha_i < 0$ and $c_g < 0$, the flow is stable.

When the spatial and the temporal amplification rates are very small, they may be related through Gaster's (1962) transformation. However, when amplification rates differ widely from zero, a separate analysis is required. It should also be observed that both temporal and spatial stability are local phenomena which validate the assumption of locally parallel flows.

If axisymmetric disturbances ($n = 0$) are considered, (3.9) becomes independent of the other equations and the eigenvalue problem can be characterized by a fourth-order equation similar to the Orr–Sommerfeld equation in parallel flows. Since $n = 1$ is expected to be the most unstable mode, we shall only consider the case of $n = 1$ in detail.

The inviscid disturbance equations are obtained by substituting $R = \infty$ in (3.4)–(3.7). The other variables are eliminated in favour of P, yielding a simple second-order equation

$$P'' + \left(\frac{1}{r} - \frac{2U'}{U-c}\right) P' - \left(\alpha^2 + \frac{n^2}{r^2}\right) P = 0$$

and the boundary conditions are $P(0) = P(\infty) = 0$.

Since the disturbance equations do not yield closed-form solutions for an arbitrary U, it is therefore necessary to resort to numerical techniques to investigate the properties of the full family of equations.

4. Solutions near $r = 0$

The boundary conditions at $r = 0$ must be supplemented by the values of the derivatives of the variables in order for it to be possible to advance the solutions by a numerical step-by-step procedure. The disturbance equations are regularly singular at $r = 0$. So the Frobenius method is used to obtain power-series solutions for the variables F, G, H and P near $r = 0$. The indicial equation has roots $\pm(n-1)$, $\pm n$ and $\pm(n+1)$, which differ by positive integers. However the nature of the equations is such as to yield three independent solutions satisfying the boundary conditions at $r = 0$ when the index $n-1$ is used. We know that two of these solutions correspond to the higher indices. The other three solutions involve logarithmic singularities and poles at $r = 0$ and so are discarded.

The radius of convergence of the power series is limited by the range in which the series expansion of U in r is valid; in the case of the jet, this radius is unity, while it is unbounded for the wake. The power series were computed numerically by programming the recursion relations. The program was designed to calculate enough terms to make the ratio of the magnitude of the last term in the series

to that of the partial sum up to that term less than a given small number. In the inviscid case, the Frobenius power-series solution corresponds to the root n of the second-order indicial equation.

5. Asymptotic solutions

The boundary conditions at infinity must be transferred to a large but finite radius for the successful application of numerical methods. The help of asymptotic solutions valid at large r is sought to achieve this. The unperturbed velocity U falls off rapidly with r and if it is considered to be zero at some large radius, the disturbance equations can be exactly solved in terms of modified Bessel functions. Then (3.4)–(3.7) can be written as

$$\alpha F + G' + G/r + nH/r = 0, \tag{5.1}$$

$$F'' + \frac{1}{r}F' - \left(\beta^2 + \frac{n^2}{r^2}\right)F - i\alpha RP = 0, \tag{5.2}$$

$$G'' + \frac{1}{r}G' - \left(\beta^2 + \frac{n^2+1}{r^2}\right)G - \frac{2n}{r^2}H + iRP' = 0, \tag{5.3}$$

$$H'' + \frac{1}{r}H' - \left(\beta^2 + \frac{n^2+1}{r^2}\right)H - \frac{2n}{r^2}G - \frac{iRnP}{r} = 0, \tag{5.4}$$

where $\beta^2 = \alpha^2 - i\alpha Rc$.

Elimination of all other variables in favour of P yields the Bessel equation

$$P'' + \frac{1}{r}P' - \left(\alpha^2 + \frac{n^2}{r^2}\right)P = 0, \tag{5.5}$$

whose solution satisfying the far boundary condition is $K_n(\alpha r)$. Equation (5.5) can be obtained more easily by taking the divergence of the incompressible Navier–Stokes equation and perturbing it. Thus, in a shearless mean flow, the pressure disturbances are not affected by the viscosity. The complete solution is given by

$$\{F, G, H, P\} = \{K_n(\alpha r), -K_n'(\alpha r)/\alpha, nK_n(\alpha r)/\alpha r, cK_n\}, \tag{5.6}$$

where a prime again denotes partial differentiation with respect to r. This solution is independent of viscosity and is often referred to as the 'non-viscous' mode.

There are two other 'viscous' modes which have no pressure component and satisfy zero boundary conditions at infinity:

$$\{F, G, H, P\} = \{K_n(\beta r), -\alpha K_n'(\beta r)/\beta^2, n\alpha K_n(\beta r)/\beta^2 r, 0\} \tag{5.7}$$

and

$$\{F, G, H, P\} = \{0, -nK_n(\beta r)/r, K_n'(\beta r), 0\}. \tag{5.8}$$

However, if U is not considered zero at a large radius, but can be expanded in a convergent or asymptotic power series in r^{-1}, more accurate asymptotic solutions can be obtained. In the case of the jet

$$U = \sum_{k=0}^{\infty} (-1)^k (k+1) r^{-(2k+4)} \quad \text{for} \quad r > 1.$$

It will be now more convenient to write the disturbance equations (3.4)–(3.7) in the form of a set of first-order equations

$$\mathbf{Y}' = \mathbf{A}(r)\,\mathbf{Y}, \tag{5.9}$$

where

$$\mathbf{Y} = \begin{bmatrix} F \\ G \\ H \\ P \\ F' \\ H' \end{bmatrix},$$

$$\mathbf{A} = \begin{bmatrix} 0 & 0 & 0 & 0 & 1 & 0 \\ -\alpha & -\frac{1}{r} & -\frac{n}{r} & 0 & 0 & 0 \\ 0 & 0 & 0 & 0 & 0 & 1 \\ 0 & -\left(\beta^2+\frac{n^2}{r^2}\right)\frac{i}{R}+\alpha U & -\frac{in}{r^2R} & 0 & -\frac{i\alpha}{R} & -\frac{in}{rR} \\ \left(\beta^2+\frac{n^2}{r^2}\right)+i\alpha RU & iRU' & 0 & i\alpha R & -\frac{1}{r} & 0 \\ 0 & \frac{2n}{r^2} & \beta^2+\frac{(n^2+1)}{r^2}+i\alpha RU & \frac{iRn}{r} & 0 & -\frac{1}{r} \end{bmatrix}.$$

Consider the case of the jet. The matrix $\mathbf{A}$ has a convergent series expansion in r^{-1} for $r > r_0$, where r_0 is large and at least greater than one, of the form

$$\mathbf{A}(r) = \sum_{k=0}^{\infty} \mathbf{A}_k r^{-k}.$$

Following Wasow (1965), uniformly asymptotic expansions for (5.9) can be obtained. $\mathbf{A}_0$ has six eigenvalues $\alpha, -\alpha, \beta, -\beta, \beta$ and $-\beta$ and has six independent eigenvectors and so can be diagonalized. In such a case, the asymptotic solutions can be written in the form

$$\mathbf{Y}(r) = e^{\mathbf{K}} r^{\mathbf{G}}\,\mathbf{Z}(r), \tag{5.10}$$

where the vector $\mathbf{Z}(r)$ has an asymptotic power-series expansion valid in an open sector S of the r plane (if r is complex) with vertex at the origin and a positive central angle not exceeding π,

$$\mathbf{Z}(r) \sim \sum_{k=0}^{\infty} \mathbf{Z}_k r^{-k}, \quad r \to \infty, \quad r \in S. \tag{5.11}$$

$\mathbf{K}$ is the diagonal matrix with eigenvalues of $\mathbf{A}_0$ as its entries. $\mathbf{G}$ also turns out to be a diagonal matrix, after formal and slightly involved calculations as given by Wasow, with each element equal to $-\frac{1}{2}$. The coefficients $\mathbf{Z}_k$ are found by formally substituting (5.10) for $\mathbf{Y}$ in (5.11) and equating coefficients of equal powers of r^{-1}.

These solutions differ in third or higher order terms from the asymptotic series of the modified Bessel function solutions previously obtained. For instance, the F component corresponding to the mode (5.7) has the power-series expansion

$$F = r^{-\frac{1}{2}} e^{-\beta r}\left\{1 + \frac{(n^2-\frac{1}{4})}{1!2}\frac{1}{\beta r} + \frac{(n^2-\frac{1}{4})(n^2-\frac{9}{4})}{2!2^2}\frac{1}{(\beta r)^2} + \left(\frac{(n^2-\frac{1}{4})(n^2-\frac{9}{4})(n^2-\frac{25}{4})}{3!2^3} + \left[\frac{i\alpha R\beta^2}{6}\right]\right)\frac{1}{(\beta r)^3} + \ldots\right\}. \quad (5.12)$$

The fourth term is corrected by the factor in square brackets and so are all the higher terms by various magnitudes. The arduous task of calculating these terms analytically was avoided by programming the recursion relations.

The formal treatment given above can be avoided by taking a cue from the asymptotic expansions for modified Bessel functions and assuming the following power-series expansions:

$$\{F, G, H, P\} = e^{\lambda r} r^m \sum_{k=0}^{\infty} \{F_k, G_k, H_k, P_k\} r^{-k}. \quad (5.13)$$

λ, m and the coefficients F_k, G_k, H_k and P_k can be obtained by the standard procedure of substitution and comparison of the powers of r^{-1}.

These refined solutions where U need not be very close to zero help in reducing the range of integration and thus saving computational time and reducing the influence of parasitic numerical errors. Also, in the case of large Reynolds number flows, it is preferable to carry the integration from outside to inside, where the additional accuracy is very much desirable. However, for small α and β, the asymptotic power series may start diverging soon and the convergent series in powers of r for modified Bessel functions will be much more useful.

The inviscid disturbance equation reduces to Bessel's equation if U is considered as zero and c is not very small as it turns out to be the case. The asymptotic solution in this case is $K_n(\alpha r)$.

6. Eigenvalue criterion

The solutions advanced by numerical integration to a large radius have to be matched to the asymptotic solutions at that radius. The matching should be such as to make the solutions and their derivatives continuous at the matching point. The set of parameters α, R, c and n that satisfies this condition is defined as the eigenvalue.

Let $\{y_i\}$, $i = 1, \ldots, 6$, represent the vector solution with the variables F, G, H, P, F' and H' as its elements. Also let $y_{i,j}, j = 1, \ldots, 3$, be the three solutions known at a large radius r_a from the integration procedure. The asymptotic solutions at r_a may be defined by $y_{i,j+3}, j = 1, \ldots, 3$. As the disturbance equations are linear, the matching condition at r_a gives

$$\sum_{j=1}^{3} C_j y_{i,j} = \sum_{j=1}^{3} C_{j+3} y_{i,j+3} \quad (i = 1, \ldots, 6), \quad (6.1)$$

where the $C_k, k = 1, \ldots, 6$, are arbitrary complex constants. Equation (6.1) is a set

of six linear algebraic equations which yield a non-trivial solution for the C_k only if

$$D(\alpha, n, c, R) = |y_{i,j}| = 0 \quad (i,j = 1 \ldots 6), \tag{6.2}$$

or in the expanded form,

$$D = \begin{vmatrix} F_1 & F_2 & F_3 & K_n(\alpha r) & K_n(\beta r) & 0 \\ G_1 & G_2 & G_3 & -\frac{K_n'(\alpha r)}{\alpha} & -\frac{\alpha}{\beta^2} K_n'(\beta r) & -\frac{n}{r} K_n(\beta r) \\ H_1 & H_2 & H_3 & \frac{n}{\alpha r} K_n(\alpha r) & \frac{n\alpha}{\beta^2 r} K_n(\beta r) & K_n'(\beta r) \\ P_1 & P_2 & P_3 & cK_n & 0 & 0 \\ F_1' & F_2' & F_3' & K_n'(\alpha r) & K_n'(\beta r) & 0 \\ H_1' & H_2' & H_3' & \frac{n}{\alpha}\left(\frac{K_n(\alpha r)}{r}\right)' & \frac{n\alpha}{\beta^2}\left(\frac{K_n(\beta r)}{r}\right)' & K_n''(\beta r) \end{vmatrix},$$

where the first three columns represent integrated vector solutions $y_{i,j}, j = 1, \ldots, 3$, $i = 1, \ldots, 6$.

We can also consider the set of algebraic equations (6.1) and satisfy all but one of the equations by fixing an arbitrary value for one of the constants. In our case, C_1 is taken as unity and the other five constants are determined numerically by solving the first five equations using the Gram–Schmidt procedure. The value of these constants is substituted in the sixth equation to yield a number, say D_1, which is used in the iteration procedure instead of D. We found that in spite of the mathematical similarity of D and D_1, the latter proved to provide a more efficient criterion for the iterative procedure. This could be because D is a relatively intricate function and could involve many undesirable differences of almost equal large numbers during computation when it is very small.

It may be noted here that matching can be carried out at any point. In the inviscid case, we integrate from outside to inside along a complex path for reasons given in the next section. The eigenvalue criterion is given by

$$(\alpha, n, c) = \begin{vmatrix} P_i & P_0 \\ P_i' & P_0' \end{vmatrix} = P_i P_0' - P_0 P_i' = 0, \tag{6.3}$$

where P_i is the Frobenius solution at the matching radius and P_0 is the integrated solution at that point.

7. Numerical techniques

The Taylor-series method was adopted to integrate the equations from near $r = 0$ to a large r where asymptotic solutions are valid. The range of integration was taken from $r = 0$ to $r = 3{\cdot}5$ in the case of the jet. At $r = 3{\cdot}5$, U is only $0{\cdot}5\,\%$ of its greatest value at the centre and can be approximated as zero. The wake profile dies out much faster and so the range was reduced to 0–$3\frac{1}{8}$, where U is only $0{\cdot}1\,\%$ of its central value. The Frobenius solutions were calculated around $r = \frac{1}{4}$ and a step size of $\frac{1}{8}$ was used to advance the solutions. It was found that in the inactive region, i.e. away from $r = 0$ and the critical layer, the step size can

be increased to $\frac{1}{5}$ or even $\frac{1}{4}$ without introducing too many additional terms in the series. The number of terms to be retained in the Taylor series was programmed to vary so as to satisfy an accuracy criterion. This criterion specified that the contribution of the last term in the series for different variables and their derivatives, like F, G, H, P, F' and H', as compared with that of the respective partial sums up to that term be less than 10^{-k} in magnitude. k was normally taken as six or seven. The above data were varied slightly according to the parameter values and test cases were run to determine optimal values.

The Newton–Raphson method was used to iterate the guessed parameters to an eigenvalue. A satisfactory convergence was considered to be achieved when consecutive iterations varied only beyond three significant digits. Newton's backward interpolation method was used to obtain the guess for an eigenvalue for a certain combination of the parameters α and R in temporal stability from two or more previously known eigenvalues with different sets of parameters. Mostly two iterations were enough to produce the required accuracy with such a scheme. The eigenvalues were frequently checked by increasing the range of integration and retaining more terms in the Taylor series, and were found to be unaffected within the limits of desired accuracy. The Reynolds number was varied up to a value of 200, where most of the stability characteristics of the viscous flow become asymptotic to those of the inviscid flow or varied slowly.

In the inviscid case, integration was carried out starting from the asymptotic values at large r towards $r = 0$ as this eliminated the possibility of the desired solutions being affected by the unwanted solution. Because of the singularity of the inviscid equation at the critical point $r = r_c$, the integration was carried along a complex path, following Lessen (1949). Since $U'(r_c) < 0$, the proper path which will give inviscid eigenvalues asymptotic to viscid eigenvalues at large R lies above the singularity.

8. Results

The critical Reynolds number and the critical wavenumber for the axisymmetric jet are found to be 37·9 and 0·40 respectively. Figure 2 shows the α, c curve for the inviscid jet flow. The instability occurs only for wavenumbers less than the neutral wavenumber, whose value, as given by Batchelor & Gill (1962) also, is 1·46. The maximum value of the amplification rate αc_i is 0·0339 at $\alpha = 0{\cdot}79$ and $c_i = 0{\cdot}0429$. The constant temporal amplification curves for the viscid jet are shown in figure 3. The curves resemble those for the most of the plane free shear layers and a lower branch definitely exists. The values of c_i at $R = 150$ and at large α are close to the corresponding inviscid values. The curves have been broken and joined with dashed lines representing the inviscid results. The lower branches of the curves tend to converge as α decreases towards zero and R increases. When α is extremely small ($\alpha \approx 0$) and R is large, the inviscid eigenvalues may not necessarily be asymptotic to the viscid eigenvalues as the related assumption of αR being large breaks down. So, the curves of inviscid instability have been discontinued near $\alpha = 0$. The incomplete dashed lines extending the lower branch indicate the probable direction in which they will

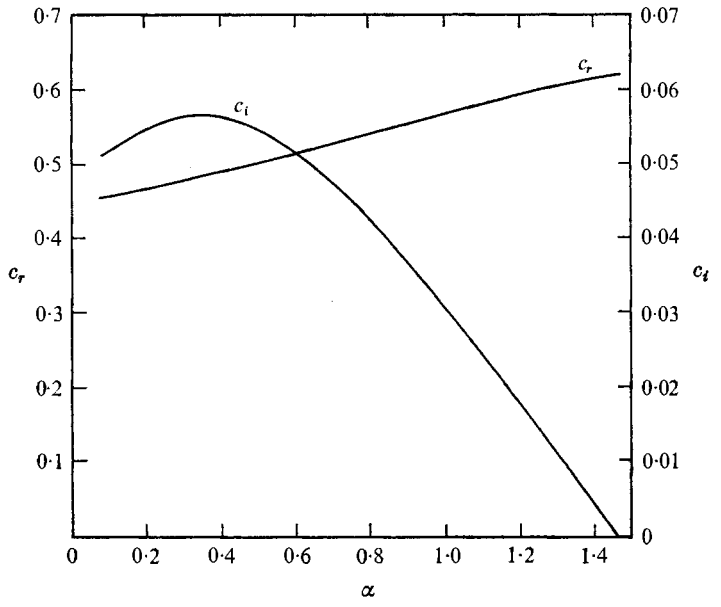

FIGURE 2. Variation of wave speed c_r and amplification factor c_i with α for the inviscid jet.

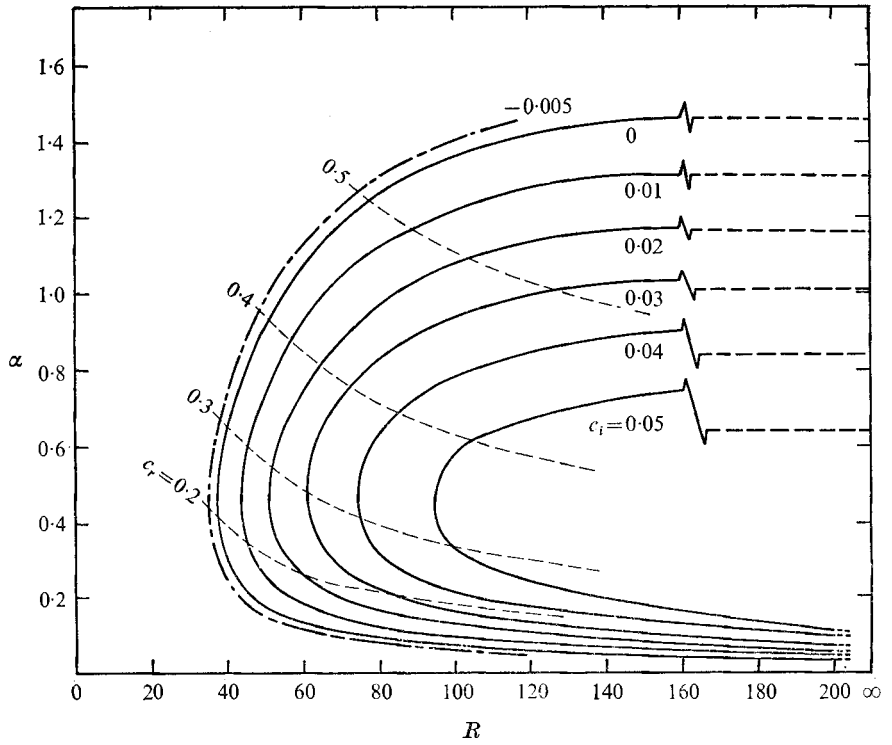

FIGURE 3. α, R plot showing constant temporal amplification (c_i = constant) and constant wave speed (c_r = constant) curves for the jet. The solid lines are broken and joined to dashed straight lines representing inviscid values.

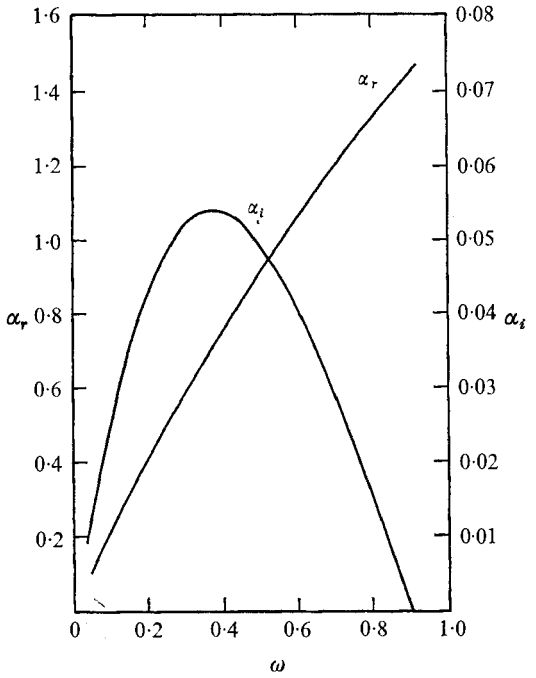

FIGURE 4. Behaviour of α_r (the real part of the wavenumber) and spatial amplification factor α_i with frequency ω for the inviscid jet.

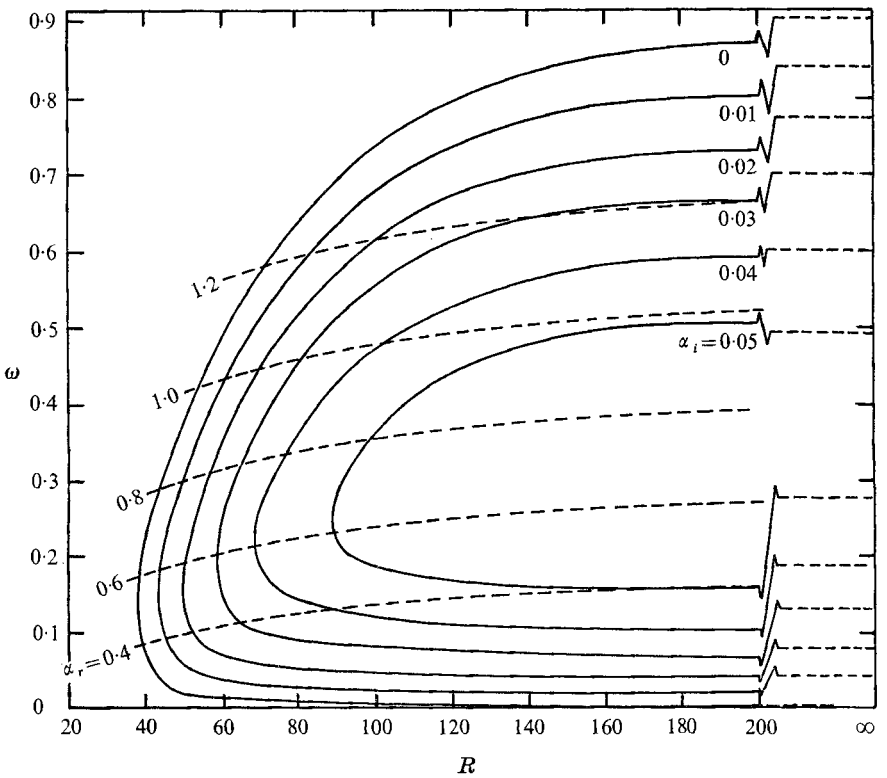

FIGURE 5. Curves of constant α_i for the jet.

proceed for still larger R. In figure 4, the real and imaginary parts α_r and α_i of the wavenumber as obtained from the spatial stability analysis of the inviscid jet are plotted against the real frequency ω. Figure 5 shows the constant spatial amplification rate (α_i = constant) curves.

It may be noticed from the figures that the viscid amplification rates (temporal or spatial) are greater than the corresponding inviscid rates for a certain range of wavenumbers. Some computations showed that the values of the former exceed the largest values of the latter. For instance, the value of c_i at $R = 150$ and $\alpha = 0{\cdot}38$ was computed as 0·06413 as opposed to the largest inviscid value of $c_i = 0{\cdot}05633$ at the same wavenumber. These results imply the existence of closed loops of constant c_i or constant α_i not shown in the figures because of lack of enough data to draw meaningful curves. The presence of these loops would seem to challenge the much stressed assumption that viscosity tends to play a stabilizing role alone in free shear layers unless a complete treatment of the problem that includes nonlinear and nonparallel effects shows otherwise. It also suggests the possibility of existence of a minor neutral stability curve as proposed by Drazin (1961) for the plane jet. However, viscosity could still tend to stabilize the flow near the inviscid region ($\alpha R = \infty$; see appendix B).

Often the length scale used in the case of the wakes is the so-called half-wake width, i.e. the distance between the point where the velocity defect has a maximum value and the point where its value is half of that. While we calculated our results on the basis of this width, we scaled them to the quarter-wake width to be consistent with the case of the jet, where the mean velocity falls off to one-quarter of the velocity at the axis in a distance equal to the length scale. Figures 6 and 7 are the plots of α, c and α, R curves for temporal stability of the wake respectively. Figures 8 and 9 represent the spatial stability characteristics of the wake in the form of ω, c and ω, R plots. These curves for the wake are smoother and indicate higher growth rates beyond the critical Reynolds number, whose value is found to be 32·6, the critical wavenumber being 0·58.

If we compare the mean velocity profiles of the jet and the wake in figure 1, we see that they closely resemble each other though the wake profile falls off more sharply away from the centre. It can be conjectured that flows with a fixed momentum flux M and profiles similar to the above will have critical Reynolds numbers (based on M) close to the values found in the present investigation. Kambe's (1969) analysis of a jet with a continuous but non-smooth parabolic profile yielded a critical Reynolds number of 32·8, which is not very different from that for the self-similar jet. However, the growth rates vary widely as the Reynolds number increases. Figure 10 shows the inviscid temporal amplification rates for the top-hat jet (from Batchelor & Gill 1962), the Poiseuille profile jet (from Kambe 1969) and for the jet and the wake profiles used in this investigation. Figures 11(*a*) and (*b*) show the real and imaginary parts of the scaled neutrally stable eigenfunction at $R = 88$ respectively. The eigenfunctions at a lower R are found to spread over larger radial distances. This is indicated by figures 12(*a*) and (*b*), where the real and imaginary parts of the scaled eigenfunctions corresponding to the minimum critical Reynolds number of the jet, $R = 37{\cdot}9$, are plotted.

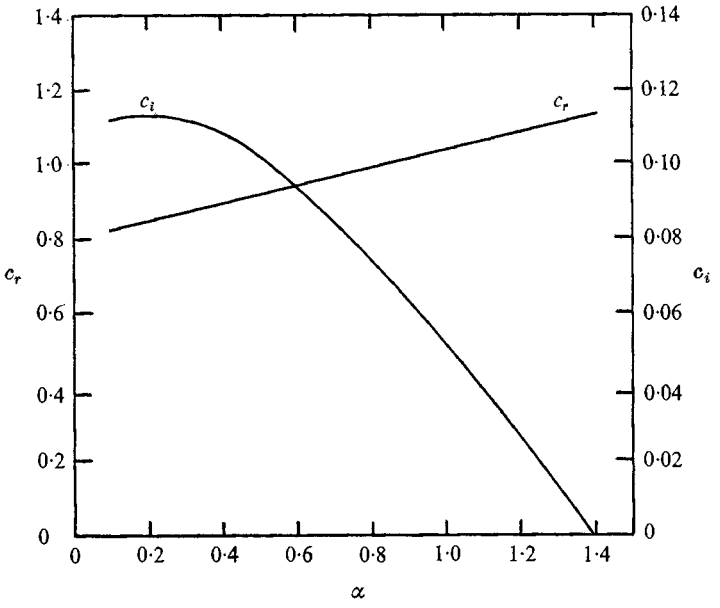

FIGURE 6. α, c plot for the inviscid wake.

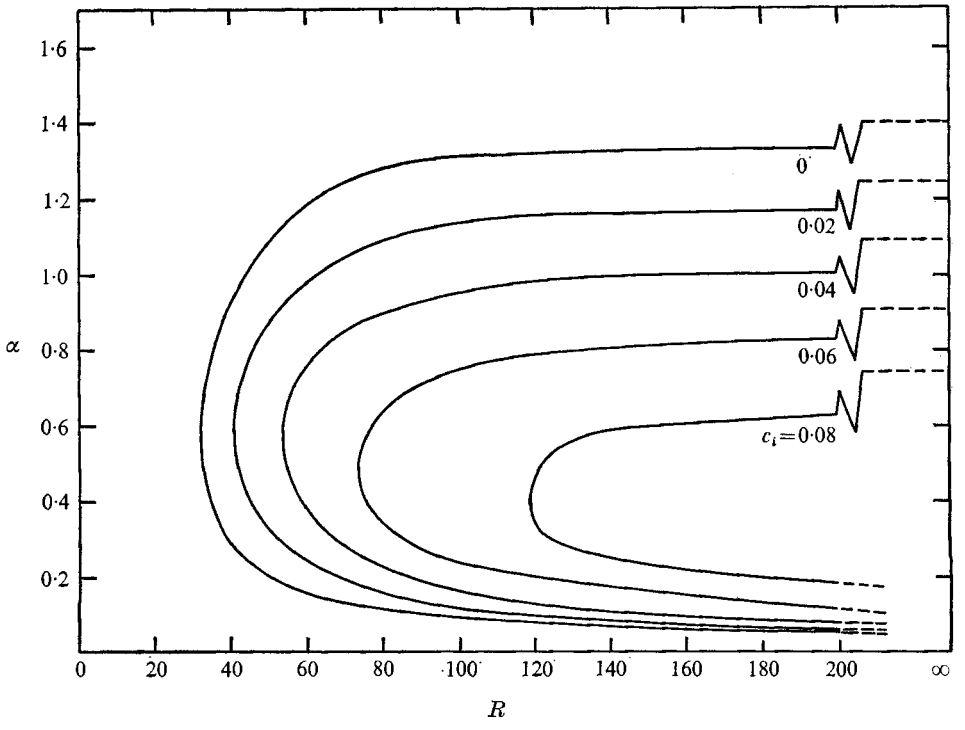

FIGURE 7. Curves of constant c_i for the wake.

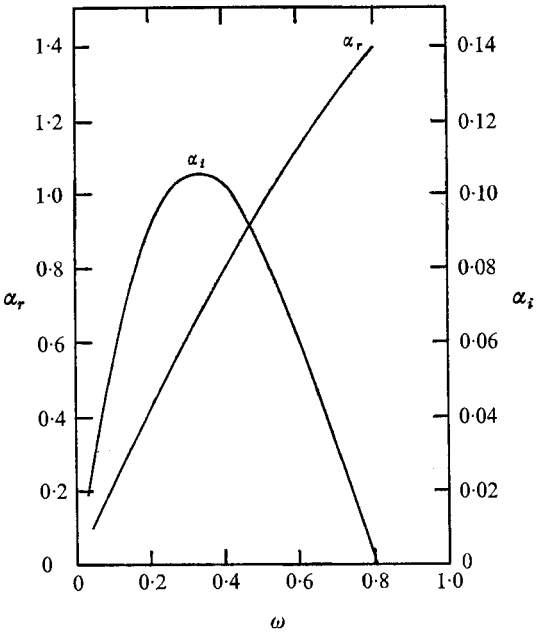

FIGURE 8. Variation of α_r and α_i with ω for the inviscid wake.

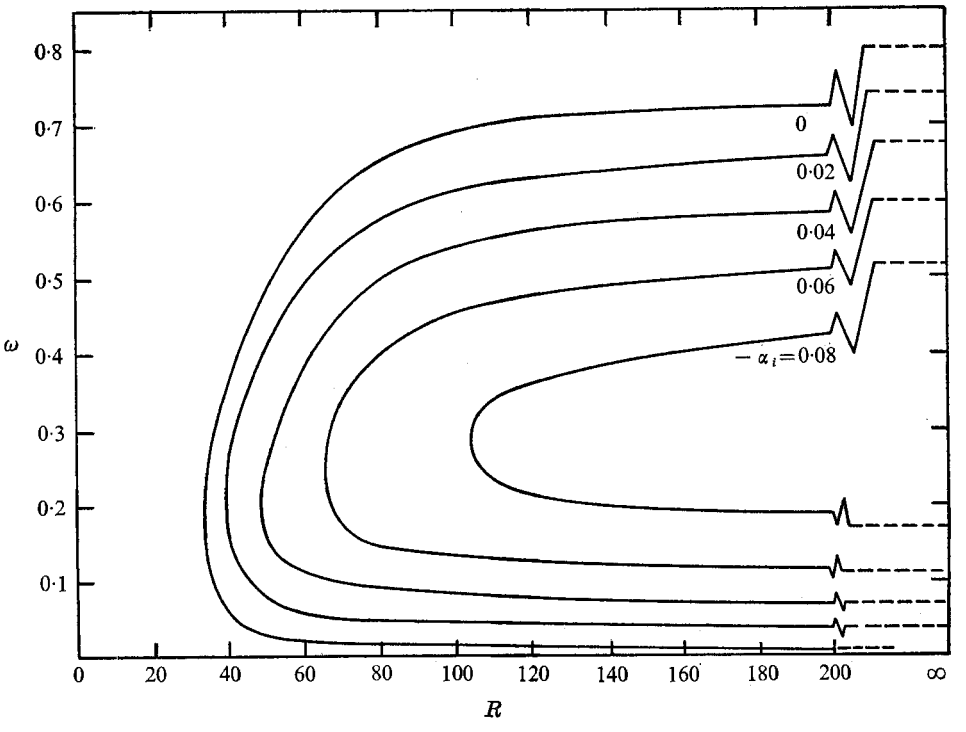

FIGURE 9. Curves of constant α_i for the wake.

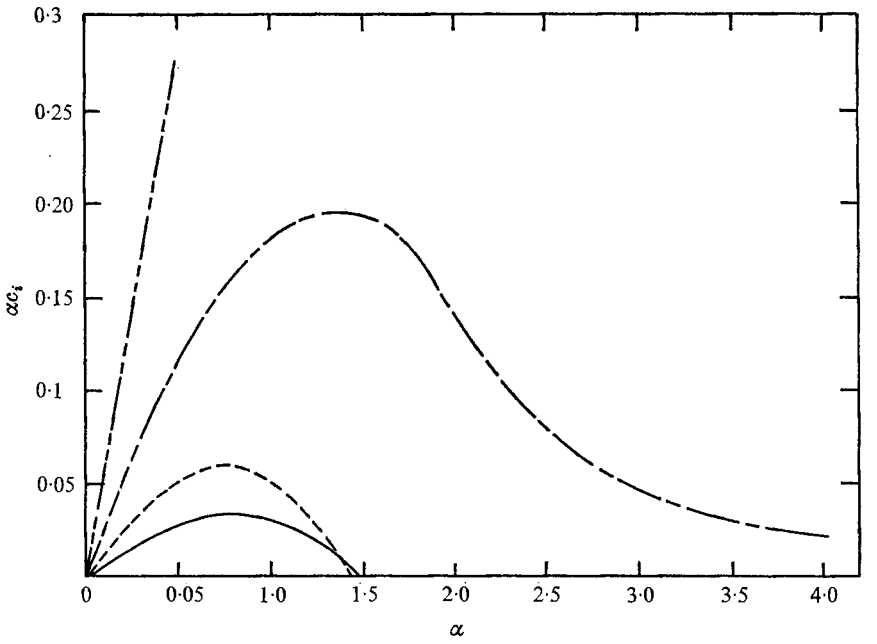

FIGURE 10. Curves of constant amplification rate αc_i for different profiles. — - - —, the top-hat jet; — · —, the parabolic profile jet; – – – –, the axisymmetric wake; ——, the axisymmetric jet.

9. Discussion

The critical Reynolds number found for the jet (37·9) does not conform with the experimental data of Reynolds (1962), who observed the development of sinuous mode at near $R = 100$. The present theoretical treatment excludes the non-parallel effects, whose role cannot be accurately guessed. Lessen & Ko (1969) approximately accounted for the effect of variational velocity and length scales in the case of the plane jet and found the results to be stabilizing. Physically it represents the dilution of the disturbance energy as the jet progresses. A similar analysis for the axisymmetric jet leaves the critical Reynolds number unchanged while that for the wake reduces it further. However, the complete effects of non-parallelism can only be accounted for by considering the two-dimensional mean velocity field to be dependent on both axial and radial co-ordinates. These effects could be considerable as the flow does not really satisfy the unidirectionality condition ($\frac{1}{8}\alpha R \gg 1$) at $R = 38$ and a non-dimensional critical wavenumber $\alpha = 0{\cdot}4$. Finite disturbances also need to be examined. At the same time, as Reynolds himself concludes, more precise experimentation is required before a final word can be said about accurate experimental values.

It appears that axisymmetric shear-layer flows are more stable than the corresponding plane shear-layer flows. The stability of plane Bickley jet has been examined by Tatsumi & Kakutani (1958) and Kaplan (1964), among many others, and the critical Reynolds number based on velocity and scale lengths not much different from those for the axisymmetric jet has been given as only

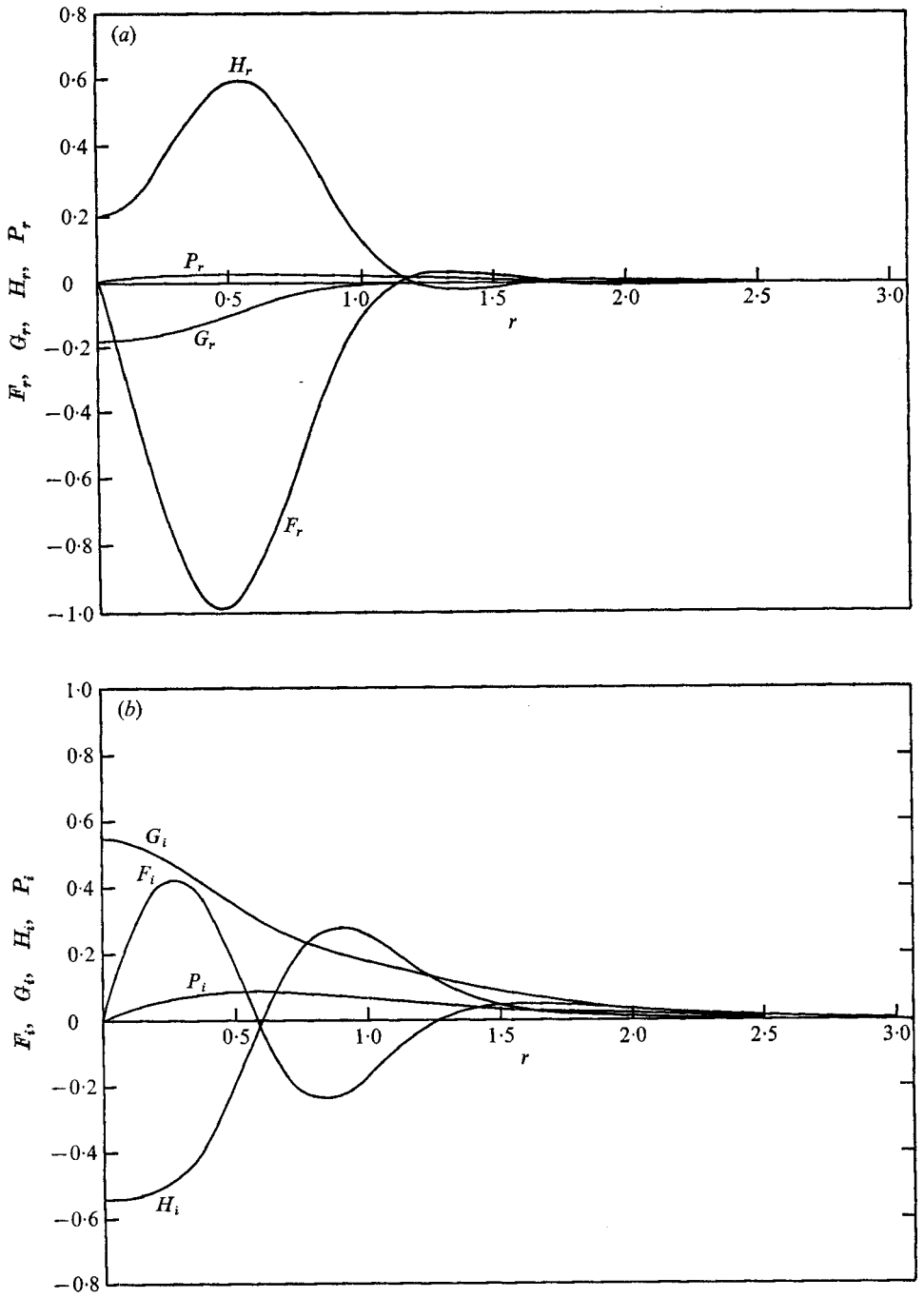

FIGURE 11. The (*a*) real and (*b*) imaginary parts of the neutrally stable eigenfunctions F, G, H and P. $R = 88$, $\alpha = 1{\cdot}3119$, $c = 0{\cdot}5214$.

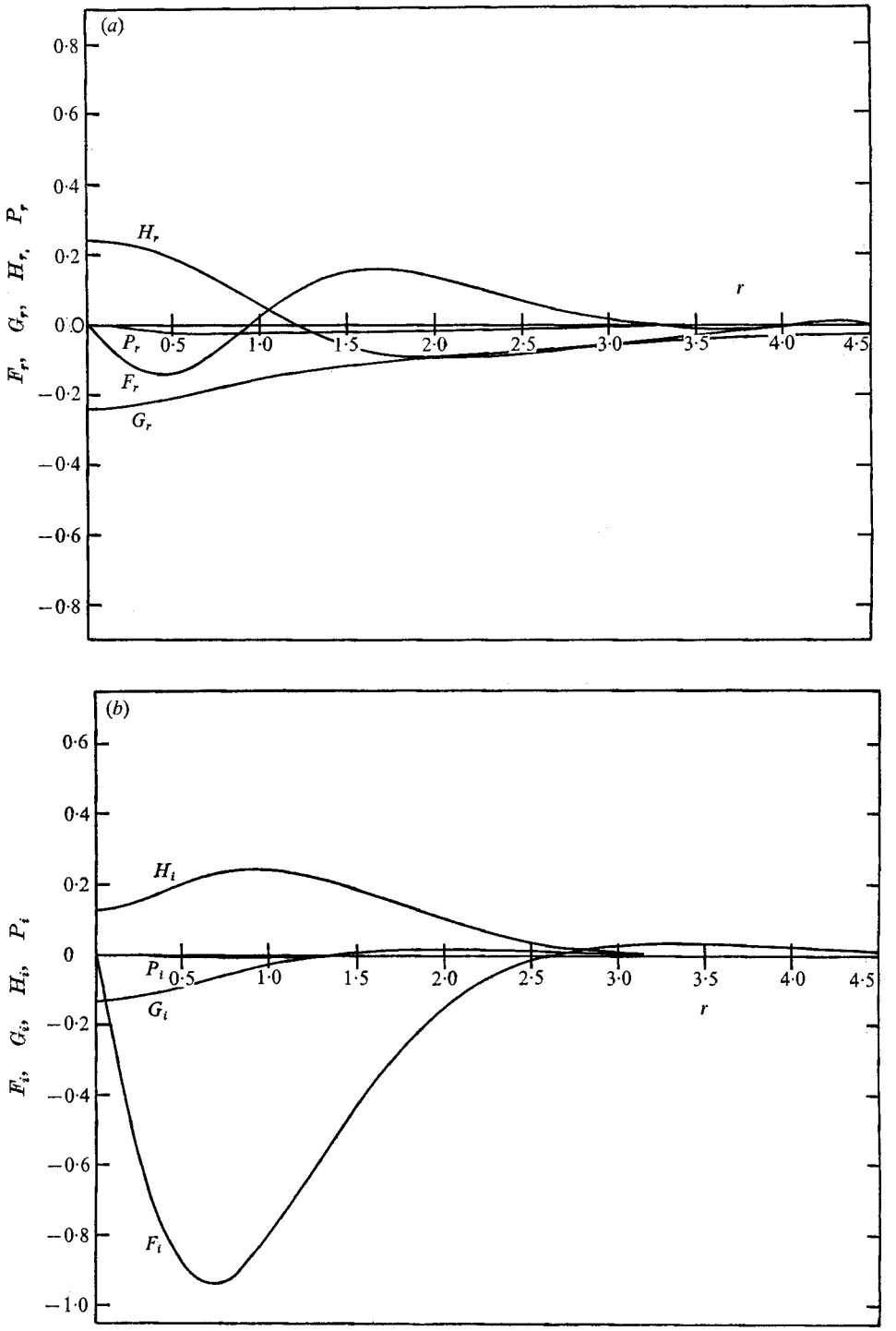

FIGURE 12. The (*a*) real and (*b*) imaginary parts of the eigenfunctions F, G, H and P at the minimum critical Reynolds number. $R = 37{\cdot}9$, $\alpha = 0{\cdot}3989$, $c = 0{\cdot}0297$.

about 4. Lessen & Ko's correction for non-parallelism raised it to near 10, which is still quite a lot smaller than that for the round jet. There does not appear to be much data to compare effectively with the results for the wake. On the basis of observations by Sato & Okada, it can be said that the amplification rate at large R should compare well with experimental measurements. It can also be expected that the critical Reynolds number for the axisymmetric wake will be much larger than that for the plane wake.

The authors acknowledge their indebtedness to the National Science Foundation for partial support of this research.

Appendix A

In § 1, it was suggested, for reasons based on physical arguments and the study of the inviscid behaviour, that only the $n = 1$ mode was likely to be most unstable. To put this argument on a solid and firm basis, some calculations were made for the $n = 0$ and $n = 2$ modes.

The $n = 0$ mode

Substituting $n = 0$ in (3.4)–(3.7), we notice that the azimuthal component of the disturbance becomes independent of the other components and the equations reduce to

$$\alpha F + G' + G/r = 0, \tag{A 1}$$

$$\alpha(U-c)F + U'G + \alpha P = \frac{1}{iR}[F'' + F'/r - \alpha^2 F], \tag{A 2}$$

$$\alpha(U-c)G - P' = \frac{1}{iR}\left[G'' + \frac{1}{r}G' - \left(\alpha^2 + \frac{1}{r^2}\right)G\right], \tag{A 3}$$

along with boundary conditions

$$F(0), P(0) \text{ finite } (F'(0) = P'(0) = 0), \quad G(0) = 0. \tag{A 4}$$

The above equations constitute a set of four first-order equations and can be reduced to one fourth-order equation analogous to the Orr–Sommerfeld equation in plane flows.

The procedure to solve the equation is similar to the one followed for the $n = 1$ mode. The Frobenius power-series solution near the axis, which satisfied the boundary conditions at $r = 0$, is calculated from the recursive relations. The asymptotic solutions can be obtained by substituting $n = 0$ in expressions in § 5. The determinant D, whose zeros give the eigenvalues, reduces to

$$D(\alpha, R, c) = \begin{vmatrix} F_1 & F_2 & K_0(\alpha r) & K_0(\beta r) \\ G_1 & G_2 & -K_0'(\alpha r)/\alpha & -(\alpha/\beta^2)K_0'(\beta r) \\ P_1 & P_2 & cK_0(\alpha r) & 0 \\ F_1' & F_2' & K_0'(\alpha r) & K_0'(\beta r) \end{vmatrix}.$$

The eigenvalues are calculated by the iterative technique detailed in § 7.

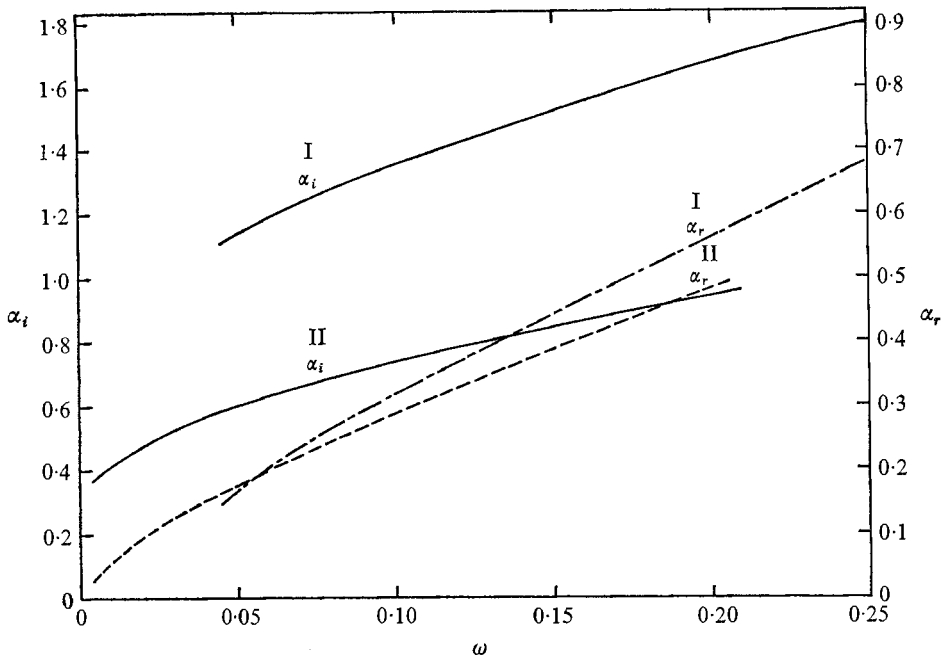

FIGURE 13. Variation of α_r and α_i with ω at $R = 75$ for the jet when $n = 0$. The two modes are distinguished by I and II.

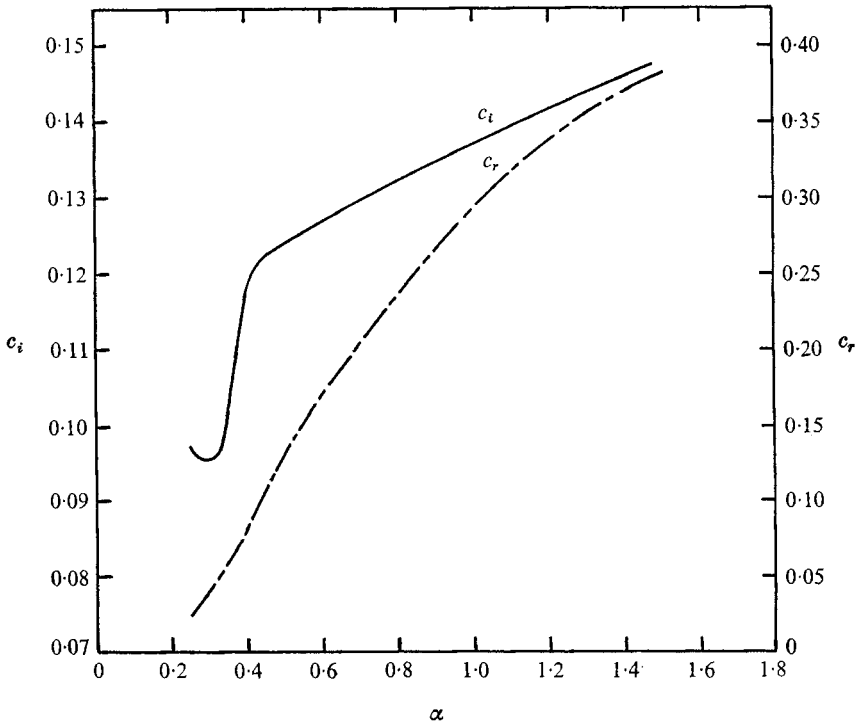

FIGURE 14. Variation of c_r and c_i with α at $R = 75$ for the jet when $n = 2$.

Sample calculations were made to examine the spatial stability of the jet. At a fixed Reynolds number $R = 75$ (double the value of the critical Reynolds number), a wide range of frequencies ω (0·005–0·025) was explored. The eigenvalues for two different modes are sketched in the curve in figure 13. Mode II is less stable than mode I but is still very highly damped. There may exist many other modes with still greater damping rates but they are of no significance. The Reynolds number was then gradually increased at a fixed frequency $\omega = 0{\cdot}005$ corresponding to the lowest calculated value of α_i.

The value of α_i decreased but still was quite large at a Reynolds number of 150 (at $R = 75$, $\alpha_i = 0{\cdot}3775$; at $R = 150$, $\alpha_i = 0{\cdot}2109$). Thus the $n = 0$ mode does not cause instability at Reynolds number in the range 0–150 and most likely is absolutely stable as there is no corresponding inviscid instability.

The $n = 2$ mode

The eigenvalues for the $n = 2$ or higher modes can be obtained by substituting the related value of n in §§ 2–6. The Frobenius power-series solutions satisfy the zero boundary conditions for the amplitudes G and H if $n > 1$.

Again, a representative calculation was made to examine the temporal stability of the jet. The eigenvalues were computed at a fixed Reynolds number of 75 with α varying from 0·2 to 1·5 (see figure 14). This mode is again highly damped with minimum c_i near $-0{\cdot}095$. There is a sharp dip in the damping rate near $\alpha = 0{\cdot}45$ but it increases again for α less than 0·3. Sample calculations were made for Reynolds numbers up to 150 and these showed no significant variation in the damping rate (for $\alpha = 0{\cdot}45$, $c_i = -0{\cdot}1223$ at $R = 75$, $c_i = -0{\cdot}1192$ at $R = 150$). As no instability exists for the inviscid case, it is likely that the $n = 2$ and the higher modes are absolutely stable.

Appendix B

In § 8, it was suggested that the α, R curves contain closed loops of constant growth rates and that there may be a minor neutrality curve in analogy with that for the plane jet proposed by Drazin.

A representative computation of eigenvalues at high Reynolds number was made to examine the above propositions and to study the behaviour of the lower branches of constant amplification rate curves. The temporal eigenvalues were computed for the case of the jet at a fixed wavenumber of 0·1 and at various Reynolds numbers progressing up to 4000. Then, with the Reynolds number fixed, the wavenumber was gradually decreased to a very small value. The numerical procedure worked efficiently; however, for Reynolds numbers greater than 2000, the orthonormalization procedure was incorporated (Conte 1964) as a precaution, the solutions being periodically orthonormalized to eliminate the disastrous effect of parasitic error destroying the linear independence of solutions.

The results are illustrated in figures 15 and 16. The temporal amplification rate c_i increases beyond the inviscid value (corresponding to the wavenumber 0·1) at a Reynolds number of approximately 260, acquires a maximum value near $R = 800$ and then gradually dips toward the inviscid value. Figure 16 shows

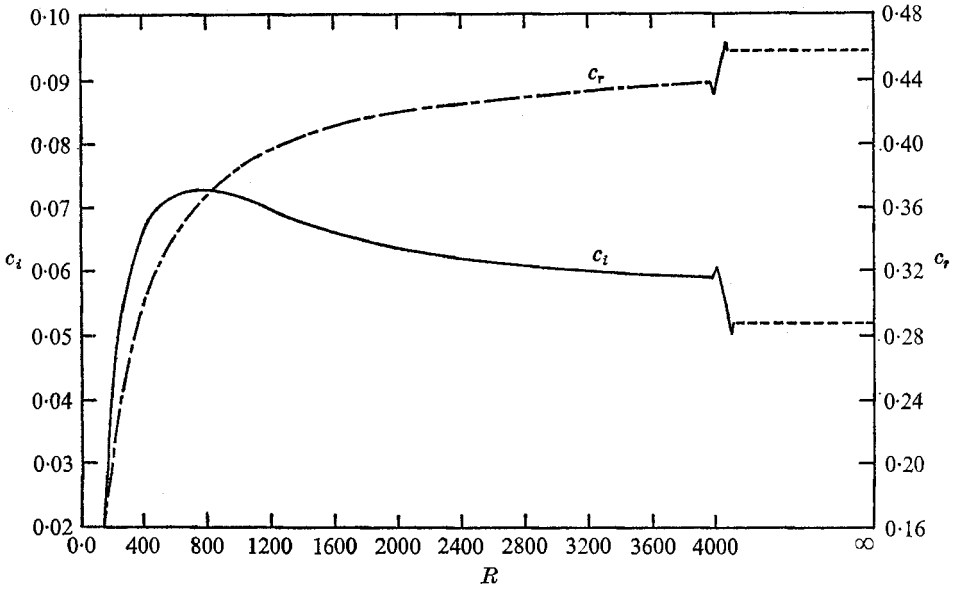

FIGURE 15. Variation of c_r and c_i with R at a constant value of $\alpha = 0{\cdot}1$ for the jet.

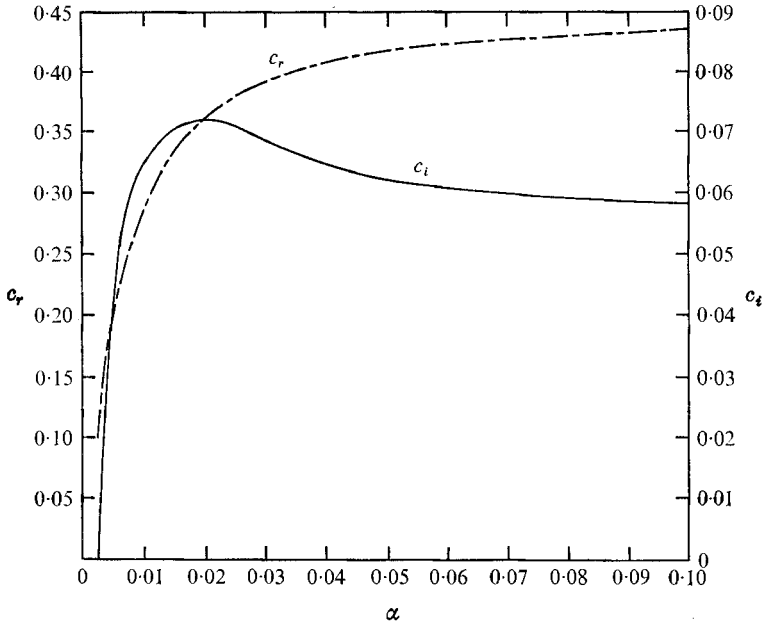

FIGURE 16. α, c curve for the viscid jet at $R = 4000$.

the variation of c_r and c_i with α as α is decreased from 0·1 to 0·002 at the fixed Reynolds number $R = 4000$. The growth rate c_i increases to a maximum value ($= 0{\cdot}0178$) at about $\alpha = 0{\cdot}0175$ and then falls sharply to zero for α near 0·002. This illustrates that the lower branches of constant growth rate curves, as is true for the other flows, keep on piling up and shifting towards $\alpha = 0$ as the Reynolds

number increases. There was no indication of a minor neutral stability curve, at least up to $R = 4000$, and its presence for the moment can be ruled out. It was also confirmed that viscosity does play a role in destabilization in at least some free flows because of the existence of viscid growth rates higher than the corresponding inviscid growth rates.

REFERENCES

BATCHELOR, G. K. & GILL, A. E. 1962 Analysis of the stability of axisymmetric jets. *J. Fluid Mech.* **14**, 529.

CONTE, S. D. 1964 The numerical solution of linear boundary-value problems. *SIAM Rev.* **8**, 309.

DRAZIN, P. G. 1961 Discontinuous velocity profiles for the Orr–Sommerfeld equation. *J. Fluid Mech.* **10**, 571.

GASTER, M. 1962 A note on the relation between temporally increasing and spatially increasing disturbances in hydrodynamic stability. *J. Fluid Mech.* **14**, 222.

GILL, A. E. 1962 On the occurrence of condensation in steady axisymmetric jets. *J. Fluid Mech.* **14**, 557.

KAMBE, T. 1969 The stability of an axisymmetric jet with parabolic profile. *J. Phys. Soc. Japan*, **26**, 566.

KAPLAN, R. E. 1964 The stability of laminar incompressible boundary layers in the presence of compliant boundaries. *M.I.T.* ASRL TR 116–1.

LANDAU, L. D. 1943 See LANDAU, L. D. & LIFSHITZ, E. M. 1959 *Fluid Mechanics*, p. 86. Pergamon.

LESSEN, M. 1949 On stability of free laminar boundary layer between parallel streams. *N.A.C.A. Tech. Rep.* no. 979.

LESSEN, M. & KO, S. H. 1969 Viscous instability of an incompressible full jet. *Phys. Fluids*, **12**, 2270.

MCNAUGHTON, K. J. & SINCLAIR, C. C. 1966 Submerged jets in short cylindrical flow vessels. *J. Fluid Mech.* **25**, 367.

RAYLEIGH, LORD 1892 See *Scientific Papers*, vol. 3, p. 575. Cambridge University Press.

REYNOLDS, A. J. 1962 Observation of a liquid-into-liquid jet. *J. Fluid Mech.* **14**, 552.

ROSENHEAD, L. 1963 *Laminar Boundary Layers*, p. 455. Oxford University Press.

SATO, H. & OKADA, O. 1966 The stability and transition of an axisymmetric wake. *J. Fluid Mech.* **26**, 237.

SCHLICHTING, H. 1955 *Boundary Layer Theory*, p. 181. McGraw-Hill.

TATSUMI, T. & KAKUTANI, T. 1958 The stability of a two-dimensional laminar jet. *J. Fluid Mech.* **4**, 261.

VILLU, A. 1962 An experimental determination of the minimum Reynolds number for instability in a free jet. *J. Appl. Mech.* **29**, 506.

WASOW, W. 1965 *Asymptotic Expansions for Ordinary Differential Equations*, p. 49. Interscience.